J Appl Electrochem (2009) 39:1017–1023
DOI 10.1007/s10800-008-9749-2

ORIGINAL PAPER

# Underscale corrosion behavior of carbon steel in a NaCl solution using a new occluded cavity cell for simulation

**Yuanliang Zhu · Yubing Qiu · Xingpeng Guo**

Received: 10 April 2008 / Accepted: 5 December 2008 / Published online: 23 December 2008


**Abstract** A new occluded corrosion cavity (OCC) simulation cell was designed to study the underscale corrosion behavior of carbon steel (N80) in 0.2 mol $L^{-1}$ NaCl solution. The chemical components of the solution in the OCC were measured and the electrochemical behavior of the occluded anode and the bulk cathode were studied by electrochemical impedance spectroscopy (EIS). The newly designed OCC cell can easily simulate the auto-catalyzing acidification process and may be used to study the mechanism of underscale corrosion. The corrosion scale exacerbates the underscale corrosion and the area ratio of the bulk cathode to the occluded anode ($R = S_c/S_a$) determines the development of simulated localized corrosion in the OCC cell. When $R$ was within a certain range, the corrosion rate in the OCC could be kept at a persistently high level. The pH of the solution in the OCC decreased and the chloride ions ($Cl^-$) concentrated as the local corrosion developed. The anodic process on the occluded anode was controlled by irreversible charge transfer and the cathodic process on the bulk cathode was controlled mainly by oxygen diffusion.

Y. Zhu · Y. Qiu · X. Guo (✉)
Department of Chemistry and Chemical Engineering, Huazhong University of Science and Technology, Hubei Key Laboratory of Materials Chemistry and Service Failure, Wuhan 430074, People's Republic of China
e-mail: guoxp@mail.hust.edu.cn

Y. Zhu
College of Biological and Chemical Engineering, Nanyang Institute of Technology, Nanyang 473066, People's Republic of China

**Keywords** Corrosion scales · Carbon steel · Underscale corrosion · Occluded corrosion cavity · EIS

## 1 Introduction

Most water transmission pipelines have a serious problem of corrosion scale deposition on the inner surface. Corrosion scales not only restrict the flow of water but also adversely affect water quality. Typical iron corrosion deposits on aged pipe surfaces are porous and have a layered structure [1–3]. Metal surfaces covered by corrosion scales have an occluded environment inside the scale. The migration of dissolved oxygen (or other oxidant species) from the bulk solution into the scale and the diffusion of iron ions, produced by a corrosion reaction, from the scale to the bulk solution are restricted. As corrosion develops, a more aggressive environment forms within the scale and accelerates corrosion under the scales.

Based on characteristics of the scale structure, underscale corrosion behavior can be described by the occluded corrosion cavity (OCC) model [4]. Underscale corrosion starts from the establishment of oxygen differential cells [5, 6] and develops continuously by an auto-catalyzing process. If the potential of the outer OCC cathode is more positive than that of the inner OCC anode the auto-catalyzing process is persistent. The corrosion rate inside the OCC is higher than that of bulk areas and these bulk areas, which act as cathodes, are thus partly or fully protected. The local corrosion rate of metals in aqueous solutions is directly affected by the degree of auto-catalysis.

Detailed studies on the auto-catalyzing process in the OCC would certainly help in understanding underscale

corrosion processes. Several OCC models have been suggested to study the local corrosion behavior of metals [4, 7–9]. For these models, however, the working electrode was often under strong polarization and the effect of the corrosion scale character on the auto-catalyzing process was hardly considered.

In this work, by considering the effect of corrosion scales, a new OCC simulated cell was designed to study the underscale corrosion behavior of carbon steel (N80) in 0.2 mol $L^{-1}$ NaCl solution. Under a coupling condition, chemical component changes in the OCC were measured and the electrochemical behavior of the occluded anode and bulk cathode was studied by electrochemical impedance spectroscopy (EIS).

## 2 Experiment

### 2.1 The OCC simulated cell and measurements of galvanic current

A schematic diagram of the newly designed OCC simulation cell is shown in Fig. 1a and a diffusion channel is shown in Fig. 1b. The whole OCC cell was made from PTFE. According to Sarin et al. [1] the simulated scale layer used in this work was a mixture of $Fe_3O_4$ (wt.25%) and $Fe_2O_3$ (wt.75%). The working electrodes, including the occluded anode and the bulk cathode, were made from N80 steel with a chemical composition of (wt.%): C 0.24, Si 0.22, Mn 1.19, P 0.013, S 0.004, Cr 0.036, Mo 0.021, Ni 0.028 and the balance was Fe. An antimony (Sb) mini-electrode and a Ag/AgCl mini-electrode [10] were used to measure the pH and the $Cl^-$ concentration of the solution in the OCC respectively. The test solution was 0.2 mol $L^{-1}$ NaCl and its pH was adjusted to 8.0 with a NaOH solution. All solutions were prepared with analytical grade reagents and distilled water.

The working electrodes were polished with emery paper to 1000 grit and then cleaned with distilled water and degreased with ethanol and acetone. The occluded electrode was mounted using a PTFE screw at the bottom of the occluded cell with an exposed area of 0.2 $cm^2$. The volume of the test solution in the OCC was about 1.5 mL. The bulk cathode which was sealed with epoxy resin had different exposure areas of 0.2, 1.0 and 2.0 $cm^2$, respectively, and was placed in the bulk solution (about 600 mL) which was exposed to air. The local corrosion cells with different area ratios of the bulk cathode to the occluded anode ($R = S_c/S_a$) were thus established in the OCC simulation cell. An auto-recording zero resistance ammeter (ZRA) was used to measure the galvanic current between the occluded anode and the bulk cathode. The potential difference between the SCE and the Sb mini-electrode as well as the Ag/AgCl mini-electrode was measured every 2 h to determine the pH and $Cl^-$ concentration of the solution in the OCC. The potentials of the occluded anode (vs. SCE and inside the OCC) and the bulk cathode (vs. SCE and in the bulk solution) were measured along with the coupling time. All the experiments were performed at room temperature and continuously for 24 h.

### 2.2 EIS measurements

EIS measurements were performed in the OCC cell shown in Fig. 1. The bulk cathode area was 1.0 $cm^2$. After the occluded anode and the bulk cathode were coupled for 0.5 h and 24 h the EIS of both electrodes was measured using a IM6e electrochemical workstation at different potentials (coupling potential $E_{cp}$ and $E_{cp} \pm 20$ mV). The frequency range was $10^4$ Hz ~ $10^{-2}$ Hz and the amplitude of the sinusoidal AC voltage signal was ±5 mV. EIS results were analyzed using Zview2 software.

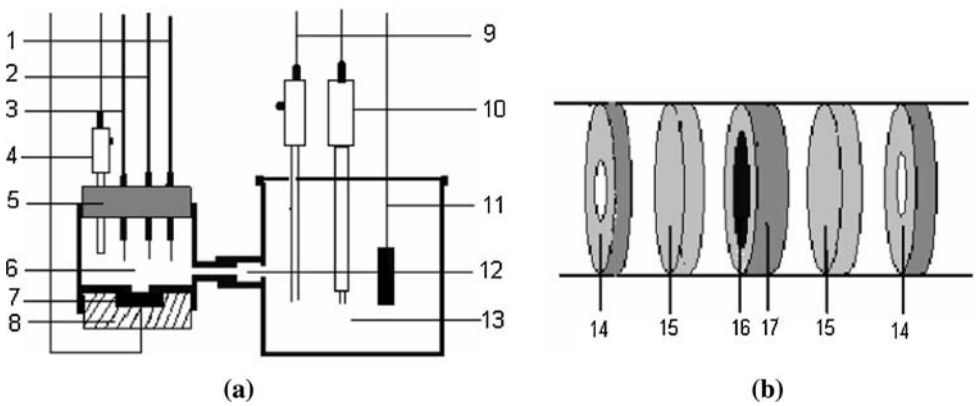


**Fig. 1** A schematic diagram of the OCC simulated cell **(a)** and diffusion channel in the OCC **(b)**. 1-platinum wire electrode, 2-Sb mini-electrode, 3-Ag/AgCl mini-electrode, 4,9-SCE, 5-rubber plug, 6-occluded cavity, 7-occluded anode, 8-PTFE screw, 10-platinum foil electrode, 11-bulk cathode, 12-diffusion channel, 13-bulk solution, 14-sealing washer, 15-filter paper, 16-simulated scale and 17-PTFE washer (Y. Zhu, Y. Qiu, X. Guo)

## 3 Results and discussion

### 3.1 The galvanic current density ($I_g$) and chemical component changes in OCC

Figure 2 shows variations of the galvanic current density ($I_g$), which is the galvanic current divided by the area of the occluded anode, with the coupling time ($t$) at different area ratios ($R = S_c/S_a$). $I_g$ did not change direction during the measurement period which indicates that the electrode in the OCC always acts as an anode and suffers corrosion. $R$ had a marked influence on the $I_g$. In Fig. 2 the $I_g$ generally fluctuates around a steady value when $R = 1$ or 5 and increases as $R$ increases from 1 to 5. Under these conditions no corrosion was observed on the bulk cathode after the experiments as shown in Fig. 3a and b. At $R = 10$ the $I_g$ was slightly larger than for $R = 5$ initially and then decreased until the end of the measurement. Under this condition some local corrosion sites were found on the bulk cathode as shown in Fig. 3c. Corrosion of the electrode in the OCC occurs as soon as the occluded condition is prevalent so that the oxygen concentration in the solution within the OCC decreases rapidly as it is consumed and is hardly replenished. While being coupled with the electrode outside the OCC, oxygen differential cells may be established, where the electrode in the OCC would act as an anode because of its more negative corrosion potential and the electrode outside the OCC could act as a cathode. Figure 2 indicates that the occlusion effect in the newly designed OCC cell started rapidly. Generally, the $I_g$ is directly proportional to $R$ and the potential difference between the bulk cathode and the occluded anode [6]. $I_g$ thus increases as $R$ increases from 1 to 5.

When $R$ increases to 10 the current density on the bulk cathode decreases markedly. New corrosion areas (anodic areas) are thus formed on the bulk cathode, as shown in Fig. 3c, and the potential becomes more negative. Figure 4 gives the potential variations of the occluded anode and the bulk cathode along with the coupling time under the coupling state ($R = 10$) in the OCC cell. The potential difference between the occluded anode and the bulk cathode falls with time and $I_g$ also decreases. The local corrosion simulation in the OCC cell may be maintained at a higher rate only when an appropriate $R$ is selected.

Based on the above results, $R = 5$ was selected for further studies. Figure 5 shows the changes in $I_g$, pH and

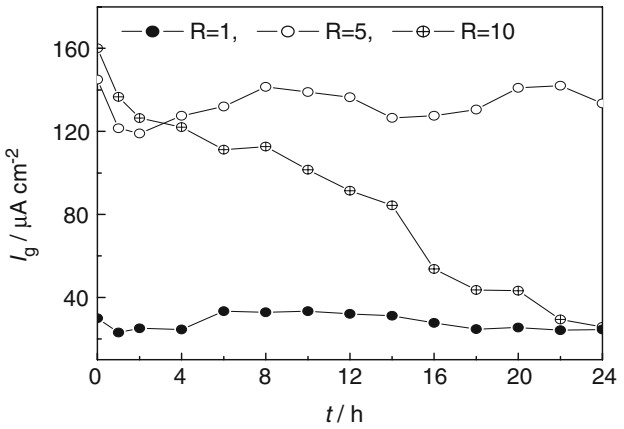


**Fig. 2** $I_g$–$t$ curves at different area ratios of the bulk cathode to the occluded anode ($R = S_c/S_a$) (Y. Zhu, Y. Qiu, X. Guo)

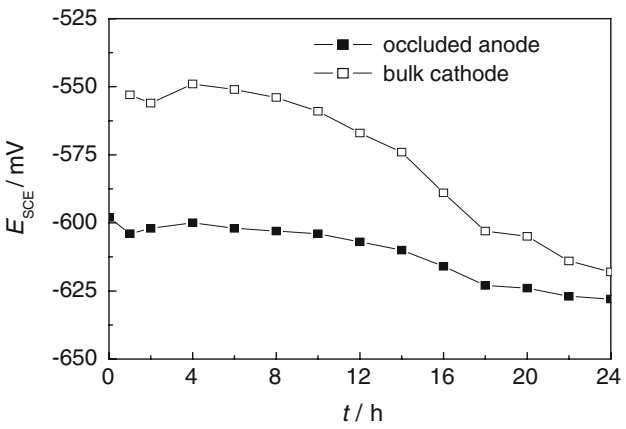


**Fig. 4** Potential variations of the occluded anode and the bulk cathode with coupling time under the coupling state in the OCC cell at $R = 10$ (Y. Zhu, Y. Qiu, X. Guo)

**Fig. 3** The corrosion morphology of the bulk cathode coupled with the occluded anode of different area ratios ($R$) after 24 h (Y. Zhu, Y. Qiu, X. Guo)

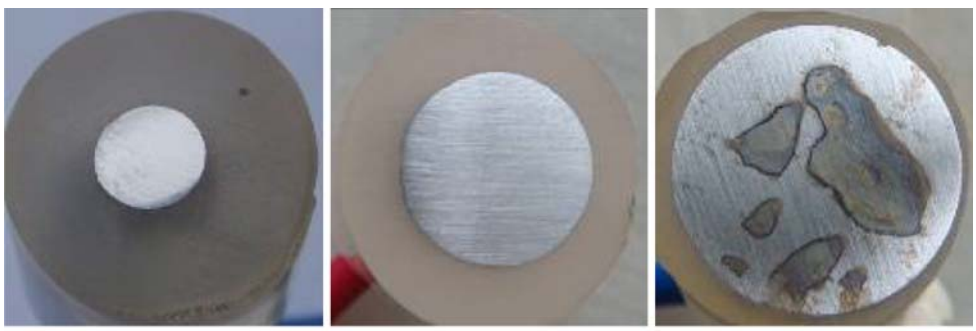

**(a)** $R$=1 **(b)** $R$=5 **(c)** $R$=10

$Cl^-$ concentration of the solution in the OCC with coupling time using different diffusion channels. One channel was filled with the simulated corrosion scale and the other was obstructed by filter paper.

As shown in Fig. 5b, the solution inside the OCC becomes more acidic and chloride ions become more concentrated as the coupling time increases. The decrease in pH is rapid early on and gradually slows after 8 h. The $Cl^-$ concentration, however, increases linearly during the whole test period. The above results may be attributed to the auto-catalyzing acidification process and its development in the OCC. Whether the diffusion channels contained the corrosion scale or not the auto-catalyzing acidification process could be simulated in the newly designed OCC cell.

The condition of the diffusion channel in the OCC cell markedly influences the auto-catalyzing acidification results. Compared with the diffusion channel obstructed by filter paper, $I_g$ was larger when it was filled with simulated corrosion scale. A decrease in pH, as well as an increase in $Cl^-$ concentration, as shown in Fig. 5, indicates that the auto-catalyzing acidification effect intensifies under this condition. The above difference might result from the physicochemical character of corrosion scales which will be discussed in a further paper by the authors. We suggest that the OCC cell and its diffusion channel, filled with appropriate simulated corrosion scales, allows for an investigation of underscale corrosion.

## 3.2 Electrochemical behavior of both electrodes

### *3.2.1 EIS of the occluded anode*

Figure 6 shows EIS results of the occluded anode under different conditions. The Nyquist plots in Fig. 6 display two similar depressed semicircles with radii that change markedly under different potentials. This shows that the slight polarization (±20 mV) versus the coupling

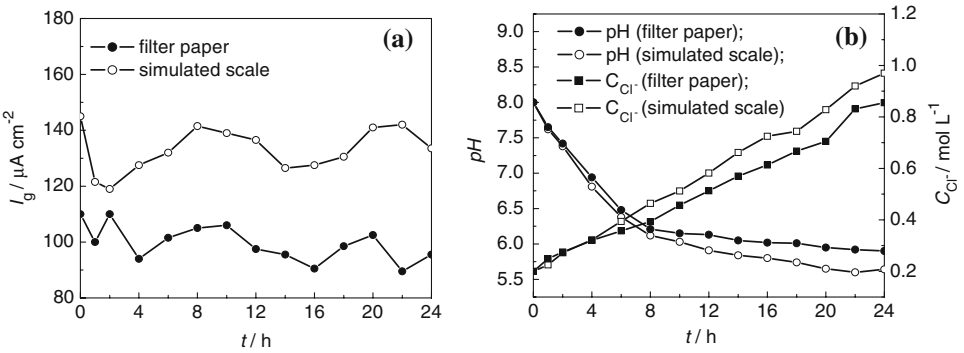


**Fig. 5** The variation of **(a)** $I_g$ and **(b)** pH and $Cl^-$ concentration of the solution in the OCC with coupling time in the OCC with different diffusion channels at $R = 5$ (Y. Zhu, Y. Qiu, X. Guo)

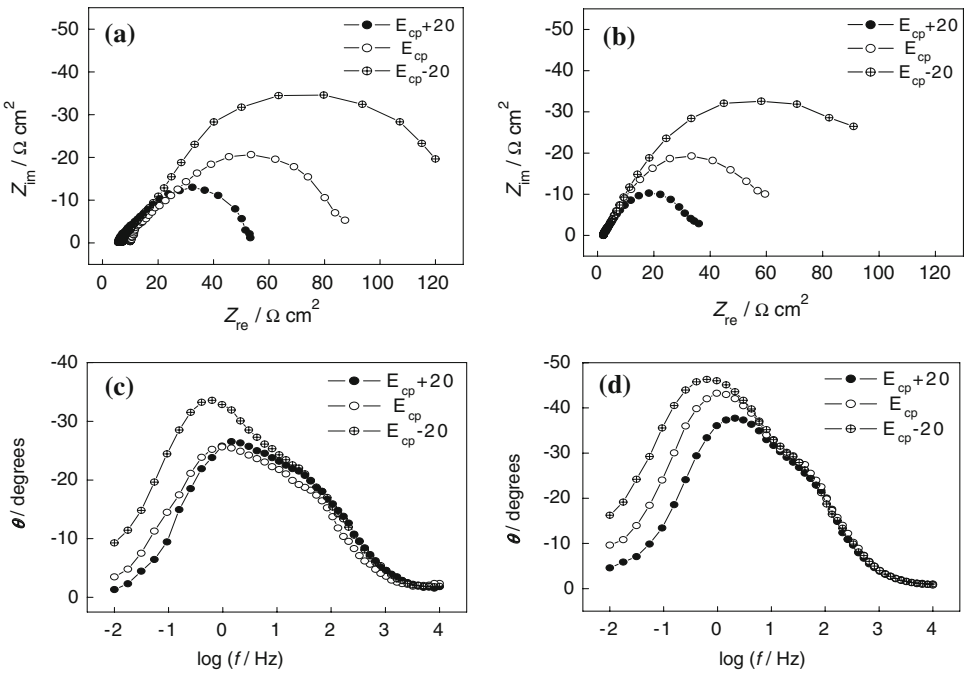


**Fig. 6** EIS diagrams for the occluded anode at different coupling times **(a)**, **(c)** 0.5 h; **(b)**, **(d)** 24 h with $R = 5$ (Y. Zhu, Y. Qiu, X. Guo)

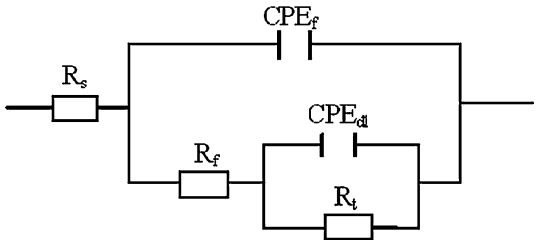


**Fig. 7** Equivalent circuit model for the occluded anode (Y. Zhu, Y. Qiu, X. Guo)

potential ($E_{cp}$) does not change the characteristic anodic process on the occluded anode but its degree of anodic polarization changes. From Fig. 6c and d two time constants are present which correspond to anodic process on the occluded anode.

Figure 7 gives an equivalent circuit model used to fit the EIS data from Fig. 6 [11–13] where $R_s$ is the solution resistance, $R_f$ is the resistance of the corrosion product layer on the occluded anode surface, $R_t$ is the charge transfer resistance and $CPE_f$ as well as $CPE_{dl}$ are constant phase elements that correspond to the corrosion product layer and the double-layer respectively. The fitting parameters obtained are summarized in Table 1.

As shown in Table 1 $R_f$ is always very small and is certainly much smaller than $R_t$ which indicates that the corrosion product layer could not prevent the anodic process. $R_s$, $R_f$, $CPE_f$ and $CPE_{dl}$ do not change with different conditions, but $R_t$ increases as the polarization potential (E) decreases. Therefore, the anodic process is controlled by an irreversible charge transfer process.

The occluded anode will dissolve continuously under the coupling state and the auto-catalyzing acidification process will occur and develop persistently. All these processes result in a change of chemical state inside the OCC and thus influence the anodic process on the occluded anode. As shown in Table 1 the values of $R_s$, $R_f$, $CPE_{dl}$ and $R_t$ all vary as the coupling time increases. The slight decrease in $R_s$ may be attributed to the increase in ionic concentration in the OCC. The decrease in $R_f$ indicates that the corrosion product layer should loosen as corrosion develops. This may be due to a decrease in pH within the OCC. This actual electrode area may also become larger and thus the $CPE_{dl}$ may increase. The decrease in $R_t$ also indicates that the active dissolution process of the occluded anode becomes easier as the coupling time increases.

### 3.2.2 *EIS of the of the bulk cathode*

Figure 8 gives the EIS results of the bulk cathode under different conditions. The Nyquist plots in Fig. 8 display similar capacitive loops in the high frequency range and a Warburg impedance in the low frequency range. These general characteristics do not change under different polarization potentials. The slight polarization (±20 mV vs. $E_{cp}$) does not change the polarization character of the cathodic process on the bulk cathode.

In the OCC cell the cathodic process on the bulk cathode consists of the reduction of dissolved oxygen ($O_2$) in the bulk solution. The oxygen diffusion process should influence the whole cathodic process. The Warburg impedance arises and varies as the degree of cathodic polarization changes. The EIS features shown in Fig. 8 can be described by an equivalent circuit given in Fig. 9 [6, 14, 15] where $R_s$ is the solution resistance, *CPE* is the constant phase element corresponding to the electric double layer, $R_t$ is the charge transfer resistance at the metal/solution interface and $Z_w$ is the Warburg impedance. Fitting parameters are listed in Table 2.

Figure 8 and Table 2 show that $R_s$ and *CPE-T* do not vary markedly with polarization potentials and coupling time. $Z_w - R$ and $R_t$ change with the polarization potential and $Z_w - R$, which describes the resistance of the $O_2$ diffusion process, was about 4–5 times larger than $R_t$. We conclude that the cathodic process on the bulk cathode should be mainly controlled by the $O_2$ diffusion process.

## 4 Conclusion

(1) A new OCC simulated cell was designed to study the underscale corrosion of N80 carbon steel in a NaCl

**Table 1** Fitting parameters obtained from EIS results in Fig. 6 (Y. Zhu, Y. Qiu, X. Guo)

| Coupling time (h) | Potentials (mV) | $R_s$ ($\Omega$ cm$^2$) | $CPE_f$ (F cm$^{-2}$) | $R_f$ ($\Omega$ cm$^2$) | $CPE_{dl}$ (F cm$^{-2}$) | $R_t$ ($\Omega$ cm$^2$) |
|---|---|---|---|---|---|---|
| 0.5 h | $E_{cp}$ + 20 | 5.5 | $3.38 \times 10^{-3}$ | 7.9 | $9.14 \times 10^{-3}$ | 42.0 |
| | $E_{cp}$ | 9.9 | $1.59 \times 10^{-3}$ | 9.4 | $9.72 \times 10^{-3}$ | 70.1 |
| | $E_{cp}$ − 20 | 7.1 | $1.91 \times 10^{-3}$ | 11.8 | $9.70 \times 10^{-3}$ | 120 |
| 24 h | $E_{cp}$ + 20 | 2.1 | $3.12 \times 10^{-3}$ | 2.9 | $1.62 \times 10^{-2}$ | 31.1 |
| | $E_{cp}$ | 2.1 | $2.14 \times 10^{-3}$ | 2.3 | $1.61 \times 10^{-2}$ | 61.2 |
| | $E_{cp}$ − 20 | 2.1 | $2.99 \times 10^{-3}$ | 2.8 | $1.71 \times 10^{-2}$ | 111 |

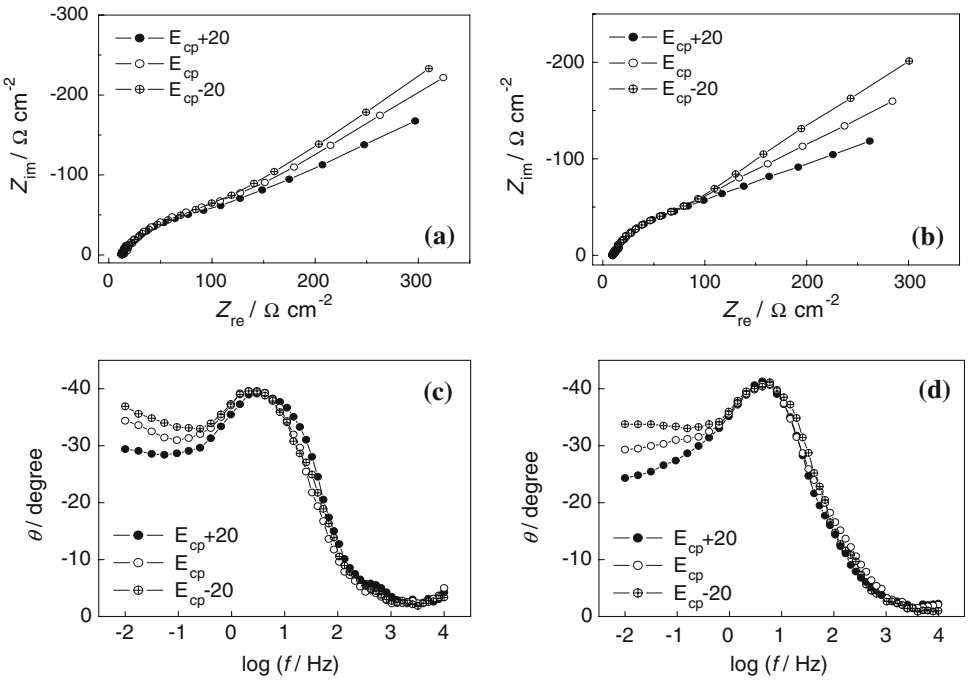


**Fig. 8** EIS diagrams for the bulk cathode at different coupling times **(a)**, **(c)** 0.5 h; **(b)**, **(d)** 24 h with $R$ = 5 (Y. Zhu, Y. Qiu, X. Guo)

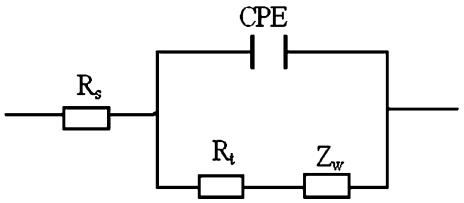


**Fig. 9** Equivalent circuit model for the bulk cathode (Y. Zhu, Y. Qiu, X. Guo)

solution. It was shown that the OCC cell could satisfactorily simulate the occlusion effect and the auto-catalyzing acidification process in underscale corrosion. It was also found to be convenient for the study of the change in solution chemical components as well as electrochemical behavior within the OCC.

(2) The area ratio of the bulk cathode to the occluded anode ($R$ = $S_c/S_a$) will determine the development of simulated local corrosion in the OCC cell. When $R$ was in a proper range the corrosion rate in the OCC could be kept at a persistently high level.

(3) The pH value of the solution in the OCC decreased and chloride ions ($Cl^-$) became more concentrated as the simulated local corrosion developed in the OCC cell. Corrosion scale accelerates the above-mentioned processes.

(4) The active dissolution process of the occluded anode was controlled by a charge transfer process and the

**Table 2** Fitting parameters obtained from EIS results in Fig. 8 (Y. Zhu, Y. Qiu, X. Guo)

| Coupling time ($t$/h) | Potentials (mV) | $R_s$ (Ω cm$^2$) | *CPE-T* (F cm$^{-2}$) | $R_t$ (Ω cm$^2$) | $Z_w$−$R$ (Ω cm$^2$ s$^{-1/2}$) | $Z_w$−T (Ω cm$^2$ s$^{-1/2}$) | $Z_w$−$P$ (Ω cm$^2$ s$^{-1/2}$) |
|---|---|---|---|---|---|---|---|
| For 0.5 h | $E_{cp}$ + 20 | 12.3 | $2.41 \times 10^{-3}$ | 101 | 576 | 103.6 | 0.41 |
| | $E_{cp}$ | 12.8 | $2.91 \times 10^{-3}$ | 134 | 701 | 83.6 | 0.48 |
| | $E_{cp}$ − 20 | 12.4 | $3.64 \times 10^{-3}$ | 145 | 884 | 104.5 | 0.48 |
| For 24 h | $E_{cp}$ + 20 | 9.3 | $2.34 \times 10^{-3}$ | 71 | 452 | 113.7 | 0.34 |
| | $E_{cp}$ | 9.4 | $3.01 \times 10^{-3}$ | 95 | 581 | 108.2 | 0.40 |
| | $E_{cp}$ − 20 | 9.2 | $3.51 \times 10^{-3}$ | 136 | 766 | 92.0 | 0.42 |

cathodic process of the bulk cathode was mainly controlled by oxygen diffusion.

**Acknowledgment** This work was financially supported by Henan Technologies Research and Development Program (No. 0524270015).

## References

1. Sarin P, Snoeyink VL, Bebee J et al (2001) Water Res 35:2961
2. Sarin P, Snoeyink VL, Lytle DA et al (2004) J Environ Eng 130:364
3. Tang ZJ, Hong SK, Xiao WZ et al (2006) Corros Sci 48:322
4. Gan Y, Li Y, Lin HC (2001) Corros Sci 43:397
5. Ijsseling FP (1989) Br Corros J 24:55
6. Cao CN (2004) In: Theories of corrosion electrochemistry. Chemical Industry, Beijing, p 100
7. Zuo JY, Jin ZQ (1982) J Chem Ind Eng 4:291
8. Lei LC, Wang FP, Gao YM et al (2001) J Mater Sci Technol 17:355
9. Ouyang WZ, Xu CC, Yue LJ et al (2004) Anti-Corros Methods Mater 51:259
10. Yan MC, Weng YJ (2004) J Chin Soc Corros Prot 24:95
11. Hong T, Sun YH, Jepson WP (2002) Corros Sci 44:101
12. Bousselmi L, Fiaud C, Tribollet B et al (1999) Electrochim Acta 44:4357
13. Marin-Cruz J, Cabrera-Sierra R, Pech-Canul Ma et al (2006) Electrochim Acta 51:1847
14. Chen Y, Hong T, Gopal M et al (2000) Corros Sci 42:979
15. Walter GW (1991) Corros Sci 32:1041